Coordinated Control Method of Voltage and Reactive Power for Active Distribution Networks Based on Soft Open Point

Peng Li, *Member, IEEE*, Haoran Ji, *Student Member, IEEE*, Chengshan Wang, *Senior Member, IEEE*, Jinli Zhao, *Member, IEEE*, Guanyu Song, Fei Ding, *Member, IEEE*, and Jianzhong Wu, *Member, IEEE*

Abstract—The increasing penetration of distributed generators (DGs) exacerbates the risk of voltage violations in active distribution networks (ADNs). The conventional voltage regulation devices limited by the physical constraints are difficult to meet the requirement of real-time voltage and VAR control (VVC) with high precision when DGs fluctuate frequently. However, soft open point (SOP), a flexible power electronic device, can be used as the continuous reactive power source to realize the fast voltage regulation. Considering the cooperation of SOP and multiple regulation devices, this paper proposes a coordinated VVC method based on SOP for ADNs. First, a time-series model of coordinated VVC is developed to minimize operation costs and eliminate voltage violations of ADNs. Then, by applying the linearization and conic relaxation, the original nonconvex mixed-integer nonlinear optimization model is converted into a mixed-integer second-order cone programming model which can be efficiently solved to meet the requirement of voltage regulation rapidity. Case studies are carried out on the IEEE 33-node system and IEEE 123-node system to illustrate the effectiveness of the proposed method.

Index Terms—Active distribution network (ADN), distributed generator (DG), mixed-integer second-order cone programming (MISOCP), soft open point (SOP), voltage and VAR control (VVC).

NOMENCLATURE

Sets

Ω_b	Set of branches without OLTC
Ω_O	Set of branches with OLTC

Variables

$P_{t,ij}, Q_{t,ij}$	Active/reactive power flow of branch ij without OLTC at period t
$P_{t,ij}^{\mathrm{OTLC}}, Q_{t,ij}^{\mathrm{OTLC}}$	Active/reactive power flow of branch ij with OLTC at period t
$I_{t,ij}, l_{t,ij}$	Current magnitude and its square of branch ij at period t
$U_{t,i}, v_{t,i}$	Voltage magnitude and its square at node i at period t
$P_{t,i}, Q_{t,i}$	Total active/reactive power injection at node i at period t
$P_{t,i}^{\mathrm{DG}}, Q_{t,i}^{\mathrm{DG}}$	Active/reactive power injection by DG at node i at period t
$P_{t,i}^{\mathrm{SOP}}, Q_{t,i}^{\mathrm{SOP}}$	Active/reactive power injection by SOP at node i at period t
$K_{t,ij}, k_{t,ij}$	Number of the tap steps and turns ratio of the OLTC connected to branch ij at period t
$Q_{t,i}^{\mathrm{CB}}$	Reactive power injection by CBs at node i at period t
$N_{t,i}^{\mathrm{CB}}$	Number of the CB units in operation at node i at period t
$P_{t,i}^{\mathrm{SOP,loss}}$	Active power losses of SOP at node i at period t
$K_{t,ij}^+, K_{t,ij}^-$	Auxiliary variables that indicate the positive/negative changes in the tap steps of the OLTC connected to branch ij at period t
$N_{t,i}^+, N_{t,i}^-$	Auxiliary variables that indicate the positive/negative changes in the number of CB units connected to node i at period t
$v_{t,ij,k}^c$	Auxiliary variable that denotes $v_{t,j} b_{t,ij,k}$
$b_{t,ij,k}$	Binary variable associated with the binary expansion scheme of $K_{t,ij}$

Parameters

N_T	Total periods of the time horizon
N_N	Total number of the nodes
Δt	Duration of each time period
$P_{t,i}^{\mathrm{L}}, Q_{t,i}^{\mathrm{L}}$	Active/reactive power consumption at node i at period t
$P_{t,i}^{\mathrm{DG,re}}$	Forecasted active power generated by DG at node i at period t
$\tan\theta_i^{\mathrm{DG}}$	$\cos\theta_i^{\mathrm{DG}}$ is the power factor of the DG at node i
$\bar{Q}_i^{\mathrm{SOP}}, \underline{Q}_i^{\mathrm{SOP}}$	Upper/lower limit of reactive power provided by SOP at node i

S_i^{SOP}	Capacity limit of SOP at node i
S_i^{DG}	Capacity limit of DG at node i
r_{ij}, x_{ij}	Resistance/reactance of branch ij
$\bar{U}, \underline{U}$	Upper/lower limit of statutory voltage range
$\bar{U}_{\mathrm{thr}}, \underline{U}_{\mathrm{thr}}$	Upper/lower limit of desired voltage range
$\bar{I}$	Upper current magnitude limit of branch
A_i^{SOP}	Loss coefficient of SOP at node i
$k_{ij,0}, \ \Delta k_{ij}$	Initial turn ratio and increment per step of OLTC connected to branch ij
$\bar{K}_{ij}$	Total steps of OLTC connected to branch ij
q_i^{CB}	Reactive power capacity of each unit of the CBs at node i
$\bar{N}_i^{\mathrm{CB}}$	Total number of CBs at node i
$W_L, \ W_V$	Weight coefficients associated with total operation costs and voltage deviation
$C_{\mathrm{loss}}, \ C_{\mathrm{tap}}, C_{\mathrm{cap}}$	Cost coefficients associated with total losses, operation of OLTC and CBs respectively
$\bar{\Delta}^{\mathrm{OLTC}}$	Maximum variation of tap steps of the OLTC in the considered time horizon
$\bar{\Delta}^{\mathrm{CB}}$	Maximum variation of the CB units in the considered time horizon

I. INTRODUCTION

RENEWABLE energy resources, in the form of distributed generators (DGs), have been integrated into distribution networks dramatically in recent years [1]. With the increasing penetration of DGs, the distribution networks have undergone a tremendous change ranging from the structure to operation mode [2], [3]. The distribution networks are gradually transforming from passive networks to active distribution networks (ADNs) comprising the role of energy collection, transmission, storage and distribution [4]. The volatile DGs and various demand-side resources begin to participate in the management of ADNs, making the operation more complex and challenging [5]. Specifically, the intermittent resources comprising wind turbines and solar photovoltaics, and controllable loads such as electric vehicles have significant uncertainties in spatial and temporal distribution, frequently leading to a sharp fluctuation of feeder power and voltage violation [6]. These disturbances cause more voltage and VAR control (VVC) problems [7], increase the operating losses and even result in stability issues of ADNs [8].

The voltage violations can be mitigated by dispatching various VAR devices. In the current distribution networks, the VVC is mainly accomplished by the regulation of primary equipment such as the on-load tap changer (OLTC), switchable capacitor banks (CBs) and tie switches, as well as the direct scheduling of the dispatchable DGs [9]. As the conventional tap adjustment of OLTC, switching of CBs and reconfiguration of tie switches are limited by the slow response and discrete voltage regulation, it is difficult to meet the requirement of real-time VVC with high precision when DGs and loads fluctuate frequently in ADNs [10]. Besides, limited by the volatile outputs and ownerships,

many dispersed DGs are still in the uneasily controllable state for the distribution system operator (DSO). The regulating capability of DGs is unable to support the centralized operation optimization.

The rapid development of power electronic technologies provides opportunities for the further optimization of ADNs operation. At distribution level, soft open point (SOP) is a power electronic device with high controllability installed to replace normally open point (NOP), realizing the flexible connection between feeders [11]. Compared to the conventional VAR regulation devices with slow response time, SOP can accurately realize the real-time active and reactive power flow control and continuous voltage regulation in the normal operation [12]. Meanwhile, due to the isolation of DC link and instantaneous control of currents, SOP can effectively contribute to the fault isolation and supply restoration of ADNs [13]. Considering the limited capability and relatively high investment of SOP, the conventional VAR regulation devices may not be completely replaced in a short term. Thus, it is of significance to realize the coordination between SOP and the other regulation devices in ADNs [14].

Previous studies have investigated the VVC problems based on the multiple regulation devices. Reference [15] developed a hybrid algorithm for the joint optimization of OLTC adjusting and CBs switching to minimize the power losses and voltage violation of distribution networks. The authors in [16] proposed a coordinated OLTC and SVC control algorithm to improve operational efficiency and a two-stage method was adopted. The problems in [15] and [16] were solved by artificial intelligence algorithms and only non-optimal solutions could be obtained in most cases. References [17] and [18] built a VAR optimization model to minimize power losses of ADNs based on second-order cone relaxation technology, which obviously improved the computation efficiency. The coordination of regulation devices on different time scales and voltage profile improvement could be further considered in this model. In [19], the active and reactive optimization involving DGs and energy storage system was conducted to achieve the minimum network loss and maximum utilization of DGs in a period of time. It was shown in [20] that SOP facilitated the economic operation of ADNs, and network performance was improved by considering both SOP and network reconfiguration. Reference [21] proposed a planning model that considers optimal investment of SOP as well as various smart technologies to alleviate the network constraints violation due to DG penetration. Considering the high investment of SOP, it is of significance to optimize the siting and sizing of SOP to realize maximum benefits in ADNs [22]. The above studies all showed that the coordination of multiple regulation devices contributed to the power losses reduction and voltage violation mitigation.

As the voltage violation frequently occurs with the fluctuation of DGs and loads, SOP rapidly adjusts the reactive power output to regulate voltage in real time. On the other hand, the switch-based devices comprising OLTC and CBs limited by security risks regulate the VAR in a long time scale. The above regulation devices can cooperate to maintain the voltage at a desired level and minimize the operation costs of ADNs.

The coordinated VVC problem not only involves the continuous transmitted active power and reactive power outputs of SOP, but also involves the discrete tap steps of OLTC and switchable units of CBs. Considering the coordination of multiple regulation devices on different time scales, the time-series optimization model is needed to be built and the real-time voltage regulation of SOP puts forward to a high requirement of optimization rapidity. But the coordinated VVC problem essentially belongs to a large-scale mixed-integer nonlinear programming (MINLP) and cannot be solved efficiently.

This paper proposes a coordinated VVC method based on SOP, improving the voltage profile while enhancing the operational efficiency of ADNs. The main contributions of this paper are summarized as follows:

1) A time-series optimization model for coordinated VVC based on SOP is developed in this paper. The proposed model considers the cooperation of SOP and multiple regulation devices to eliminate voltage violations while minimizing the operation costs of ADNs.

2) By applying the linearization and conic relaxation, the original MINLP model is converted into the mixed-integer second-order cone programming (MISOCP) model, which can be efficiently solved to meet the demands of optimization rapidity with the real-time voltage regulation of SOP.

The remainder of the paper is organized as follows. Section II builds the coordinated VVC model based on SOP of ADNs. The original problem is converted into an MISOCP model by using the linearization and conic relaxation in Section III. Case studies are given in Section IV to verify the effectiveness of the proposed method using two IEEE test systems. Section V concludes this paper with a discussion.

II. COORDINATED VVC PROBLEM FORMULATION BASED ON SOP

Considering the cooperation of multiple VAR regulation devices, the SOP-based coordinated VVC model is built in this section. SOP adjusts the active and reactive power flow in real time, rapidly responding to the voltage volatility caused by DGs. Accounting for the response rate and security reasons, the switching devices comprising OLTC and CBs regulate the VAR in a long time scale to avoid frequent actions. The multiple VAR regulation devices are coordinated to maintain the system voltage within a desired range while improving the operational efficiency of ADNs by using the voltage interval control strategy. When the voltage violation occurs, it is effectively mitigated by the coordination of above VAR regulation devices, ensuring the secure operation level of system.

A. Principle and Modelling of SOP

SOP is installed between the adjacent feeders to replace NOP in ADNs [11], as shown in Fig. 1. Compared with traditional switching operation, SOP can precisely control the active and reactive power flow with lower operation costs, and avoid the risk caused by the frequent switching actions. In this paper, the
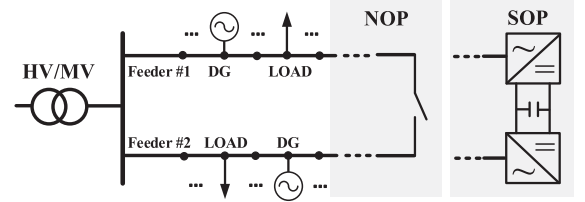

Fig. 1. Schematic of SOP installation.

active power and reactive power of SOP are scheduled by a centralized manner and the control signals of SOP are transmitted by the fast telecommunications, such as fiber-optic communication or private wireless network communication.

SOP is mainly based on fully controlled power electronic devices. This paper uses back-to-back voltage source converters (B2B VSC) to analyze the optimization model for SOP in the steady state [12], and $PQ - V_{dc}Q$ control is selected as the SOP control mode. The controllable variables for SOP comprise the active and reactive power outputs of the two converters. Although the efficiency of B2B VSC is sufficiently high, it inevitably produces losses when the large-scale power transfer occurs. As for the reactive power outputs, the two converters are independent of each other because of DC isolation, only required to meet its own capacity constraints. Then the model of SOP is obtained, containing the following constraints.

1) *SOP active power constraints:*

$$P_{t,i}^{SOP} + P_{t,j}^{SOP} + P_{t,i}^{SOP,loss} + P_{t,j}^{SOP,loss} = 0 \quad (1)$$

$$P_{t,i}^{SOP,loss} = A_i^{SOP} \sqrt{\left(P_{t,i}^{SOP}\right)^2 + \left(Q_{t,i}^{SOP}\right)^2} \quad (2)$$

$$P_{t,j}^{SOP,loss} = A_j^{SOP} \sqrt{\left(P_{t,j}^{SOP}\right)^2 + \left(Q_{t,j}^{SOP}\right)^2} \quad (3)$$

2) *SOP reactive power constraints:*

$$\underline{Q}_i^{SOP} \leq Q_{t,i}^{SOP} \leq \bar{Q}_i^{SOP} \quad (4)$$

$$\underline{Q}_j^{SOP} \leq Q_{t,j}^{SOP} \leq \bar{Q}_j^{SOP} \quad (5)$$

3) *SOP capacity constraints:*

$$\sqrt{\left(P_{t,i}^{SOP}\right)^2 + \left(Q_{t,i}^{SOP}\right)^2} \leq S_i^{SOP} \quad (6)$$

$$\sqrt{\left(P_{t,j}^{SOP}\right)^2 + \left(Q_{t,j}^{SOP}\right)^2} \leq S_j^{SOP} \quad (7)$$

B. Modelling of the Coordinated VVC Based on SOP

1) Objective Function: Accounting for the operational efficiency and voltage profile of ADNs, the linear weighted combination of minimum total operational cost and minimum voltage deviation is proposed as the objective function in this paper, which is formulated as:

$$\min f = W_L \left(f_{loss} + f_{switch} \right) + W_V f_V \quad (8)$$

Where the weight coefficients W_L and W_V of each term in (8) can be determined by using the analytic hierarchy process (AHP) in [23]. The total system operational costs consist of two parts, namely the cost of power losses f_{loss} and the cost of switching operation f_{switch}.

The overall costs of active power losses involve the network losses and the power losses caused by the power transmission of SOP.

$$f_{\text{loss}} = C_{\text{loss}}\left(\sum_{t=1}^{N_T}\sum_{ij\in\Omega_b} r_{ij}I_{t,ij}^2\Delta t + \sum_{t=1}^{N_T}\sum_{i=1}^{N_N} P_{t,i}^{\text{SOP,loss}}\Delta t\right) \tag{9}$$

The overall costs of switching operation are composed of the adjusting cost of OLTC and the switching cost of CBs.

$$f_{\text{switch}} = \sum_{ij\in\Omega_O}\sum_{t=1}^{N_T}\left(C_{\text{tap}}\left|K_{t,ij} - K_{t-1,ij}\right|\right)$$
$$+ \sum_{i=1}^{N_N}\sum_{t=1}^{N_T}\left(C_{\text{cap}}\left|N_{t,i}^{\text{CB}} - N_{t-1,i}^{\text{CB}}\right|\right) \tag{10}$$

The extent of voltage deviation f_V are formulated as follows.

$$f_V = \sum_{t=1}^{N_T}\sum_{i=1}^{N_N}\left|U_{t,i}^2 - \tilde{U}^2\right| : (U_{t,i} \geq \bar{U}_{\text{thr}} || U_{t,i} \leq \underline{U}_{\text{thr}}) \tag{11}$$

Where $\tilde{U}$ denotes the desired range of voltage magnitude. Equation (11) indicates the threshold function reflecting the extent of voltage deviation [24]. The voltage interval control strategy is adopted to maintain the voltage at the desired level. First of all, it is essential to maintain the voltage within the statutory range $[\underline{U}, \bar{U}]$. If the voltage magnitude $U_{t,i}$ is within the desired range $[\underline{U}_{\text{thr}}, \bar{U}_{\text{thr}}]$, namely the margin of threshold, the objective function only involves minimization of total operation costs. While the voltage magnitude is going out of the desired range, the term f_V will take effect to minimize the extent of deviation from the desired range.

The constraints mainly include the operation constraints of distribution networks and the operation constraints of VAR regulation devices, as described next.

2) System Operation Constraints: The Distflow branch model, proposed in [25], is used for modelling the distribution networks. It can be described mathematically as the following constraints:

$$\sum_{ji\in\Omega_b}\left(P_{t,ji} - r_{ji}I_{t,ji}^2\right) + P_{t,i} + \sum_{ji\in\Omega_O} P_{t,ji}^{\text{OTLC}}$$
$$= \sum_{ik\in\Omega_b} P_{t,ik} + \sum_{ik\in\Omega_O} P_{t,ik}^{\text{OTLC}} \tag{12}$$

$$\sum_{ji\in\Omega_b}\left(Q_{t,ji} - x_{ji}I_{t,ji}^2\right) + Q_{t,i} + \sum_{ji\in\Omega_O} Q_{t,ji}^{\text{OTLC}}$$
$$= \sum_{ik\in\Omega_b} Q_{t,ik} + \sum_{ik\in\Omega_O} Q_{t,ik}^{\text{OTLC}} \tag{13}$$

$$U_{t,i}^2 - U_{t,j}^2 - 2\left(r_{ij}P_{t,ij} + x_{ij}Q_{t,ij}\right) + \left(r_{ij}^2 + x_{ij}^2\right)I_{t,ij}^2 = 0 \tag{14}$$

$$I_{t,ij}^2 U_{t,i}^2 = P_{t,ij}^2 + Q_{t,ij}^2 \tag{15}$$

$$P_{t,i} = P_{t,i}^{\text{DG}} + P_{t,i}^{\text{SOP}} - P_{t,i}^{\text{L}} \tag{16}$$

$$Q_{t,i} = Q_{t,i}^{\text{DG}} + Q_{t,i}^{\text{SOP}} + Q_{t,i}^{\text{CB}} - Q_{t,i}^{\text{L}} \tag{17}$$

Constraints (12) and (13) represent the active and reactive power balance of node i at period t, respectively. The Ohm's law over branch ij at period t is expressed as (14). The current magnitude of each line can be determined by (15). Constraints (16) and (17) indicate the total active and reactive power injection of node i at period t, respectively.

The security constraints of ADNs are expressed as follows:

$$(\underline{U})^2 \leq U_{t,i}^2 \leq (\bar{U})^2 \tag{18}$$

$$I_{t,ij}^2 \leq (\bar{I})^2 \tag{19}$$

Constraint (18) denotes the system voltage limits. The maximum line current capacity is formulated as (19).

3) DG Operation Constraints:

$$P_{t,i}^{\text{DG}} = P_{t,i}^{\text{DG,re}} \tag{20}$$

$$Q_{t,i}^{\text{DG}} = P_{t,i}^{\text{DG}}\tan\theta_i^{\text{DG}} \tag{21}$$

$$\sqrt{\left(P_{t,i}^{\text{DG}}\right)^2 + \left(Q_{t,i}^{\text{DG}}\right)^2} \leq S_i^{\text{DG}} \tag{22}$$

Constraint (20) assumes that the active power generated by DGs is equal to the forecasted value. Constraint (21) denotes the reactive power constraint of DGs and the capacity constraint of DGs is expressed as (22).

4) OLTC Operation Constraints:

$$U_{t,i} = k_{t,ij} U_{t,j} \tag{23}$$

$$k_{t,ij} = k_{ij,0} + K_{t,ij}\Delta k_{ij} \tag{24}$$

$$\sum_{t=1}^{N_T}\left|K_{t,ij} - K_{t-1,ij}\right| \leq \bar{\Delta}^{\text{OLTC}} \tag{25}$$

$$-\bar{K}_{ij} \leq K_{t,ij} \leq \bar{K}_{ij}, \; K_{t,ij} \in \mathbb{Z} \tag{26}$$

Constraints (23) and (24) define the relationship between the regulated voltage and the tap steps of OLTC. Constraint (25) limits the maximum variation of the tap steps during the considered time horizon. Constraint (26) represents the variation range of the discrete tap steps.

5) CBs Operation Constraints:

$$Q_{t,i}^{\text{CB}} = N_{t,i}^{\text{CB}} \times q_i^{\text{CB}} \tag{27}$$

$$\sum_{t=1}^{N_T}\left|N_{t,i}^{\text{CB}} - N_{t-1,i}^{\text{CB}}\right| \leq \bar{\Delta}^{\text{CB}} \tag{28}$$

$$0 \leq N_{t,i}^{\text{CB}} \leq \bar{N}^{\text{CB}}, \; N_{t,i}^{\text{CB}} \in \mathbb{Z} \tag{29}$$

Constraint (27) denotes the total reactive power injected by CBs. Constraint (28) limits the maximum variation of CB units in operation during the considered time horizon.

The variables in this model not only involve the continuous active and reactive power outputs of SOP, but also involve the discrete tap steps of OLTC and switchable units of CBs. As a consequence, (1)–(29) form the coordinated VVC model based on SOP. Accounting for the time-series characteristics of the model, the dimension of VVC problem has a rapid increasing with more time periods. It is essentially a large-scale MINLP problem, requiring to be solved accurately and efficiently.

III. MISOCP MODEL CONVERSION

The aforementioned SOP-based coordinated VVC problem cannot be solved by the existing method efficiently. In this section, using the linearization and conic relaxation, the original model is transmitted into an MISOCP model to realize a rapid and accurate calculation.

A. Standard Form of Conic Programming

Second-order cone programming (SOCP) mathematically belongs to convex programming, which can be regarded as the generalization of both linear and nonlinear programming [26]. As SOCP has excellent performance of global optimality and computation efficiency, it has been widely used in solving MINLP problems. The standard form can be written as [27]:

$$\min\{\boldsymbol{c}^{\mathrm{T}}\boldsymbol{x}|\boldsymbol{A}\boldsymbol{x} = \boldsymbol{b}, \boldsymbol{x} \in \boldsymbol{K}\} \tag{30}$$

Where $\boldsymbol{x}$ is the decision variables. $\boldsymbol{c}$, $\boldsymbol{b}$ and $\boldsymbol{A}$ are the constant vectors and matrix. $\boldsymbol{K}$ denotes the Cartesian product of a nonempty-pointed convex cone, which is generally expressed as the quadratic cone (31) or rotated quadratic cone (32).

$$\boldsymbol{K}_1 = \left\{ \boldsymbol{x} \in R^n : x_1 \geq \sqrt{\sum\nolimits_{j=2}^{n} x_j^2},\ x_1 \geq 0 \right\} \tag{31}$$

$$\boldsymbol{K}_2 = \left\{ \boldsymbol{x} \in R^n : 2x_1 x_2 \geq \sqrt{\sum\nolimits_{j=3}^{n} x_j^2},\ x_1, x_2 \geq 0 \right\} \tag{32}$$

As shown above, SOCP has notably strict demands on the mathematical formulation. The objective function must be a linear function of the decision variables $\boldsymbol{x}$, and its feasible region is composed of linear equality constraints and convex cone constraints. Therefore, the original nonconvex MINLP model must be reformulated in advance before applying SOCP.

B. Conversion to an MISOCP Model

Constraints (9), (12)–(15) and (18) and (19) have the square representation of the voltage magnitude and current amplitude. Firstly, it needs to use variable substitution to realize the linearization, namely let $v_{t,i}$ and $l_{t,ij}$ denote the $U_{t,i}^2$ and $I_{t,ij}^2$.

Linearized constraints are expressed as follows:

$$f_{\mathrm{loss}} = C_{\mathrm{loss}} \left(\sum_{t=1}^{N_T} \sum_{ij \in \Omega_b} r_{ij} l_{t,ij} \Delta t + \sum_{t=1}^{N_T} \sum_{i=1}^{N_N} P_{t,i}^{\mathrm{SOP,loss}} \Delta t \right) \tag{33}$$

$$\sum_{ji \in \Omega_b} (P_{t,ji} - r_{ji} l_{t,ij}) + P_{t,i} + \sum_{ji \in \Omega_O} P_{t,ji}^{\mathrm{OTLC}}$$
$$= \sum_{ik \in \Omega_b} P_{t,ik} + \sum_{ik \in \Omega_O} P_{t,ik}^{\mathrm{OTLC}} \tag{34}$$

$$\sum_{ji \in \Omega_b} (Q_{t,ji} - x_{ji} l_{t,ij}) + Q_{t,i} + \sum_{ji \in \Omega_O} Q_{t,ji}^{\mathrm{OTLC}}$$
$$= \sum_{ik \in \Omega_b} Q_{t,ik} + \sum_{ik \in \Omega_O} Q_{t,ik}^{\mathrm{OTLC}} \tag{35}$$

$$v_{t,i} - v_{t,j} - 2 (r_{ij} P_{t,ij} + x_{ij} Q_{t,ij}) + (r_{ij}^2 + x_{ij}^2) l_{t,ij} = 0 \tag{36}$$

$$(\underline{U})^2 \leq v_{t,i} \leq (\bar{U})^2 \tag{37}$$

$$l_{t,ij} \leq (\bar{I})^2 \tag{38}$$

After substituting the variable, (15) continues to be nonlinear due to the quadratic term. It can be relaxed to the following second-order cone constraint [28], [29]:

$$\left\| [2P_{t,ij}\ 2Q_{t,ij}\ l_{t,ij} - v_{t,i}]^{\mathrm{T}} \right\|_2 \leq l_{t,ij} + v_{t,i} \tag{39}$$

The operation constraints of SOP in (2)–(3) and (6)–(7) as well as capacity constraint of DGs in (22) are all quadratic nonlinear constraints, which can be transformed into the following rotated quadratic cone constraints:

$$\left(P_{t,i}^{\mathrm{SOP}}\right)^2 + \left(Q_{t,i}^{\mathrm{SOP}}\right)^2 \leq 2 \frac{P_{t,i}^{\mathrm{SOP,loss}}}{\sqrt{2}A_i^{\mathrm{SOP}}} \frac{P_{t,i}^{\mathrm{SOP,loss}}}{\sqrt{2}A_i^{\mathrm{SOP}}} \tag{40}$$

$$\left(P_{t,j}^{\mathrm{SOP}}\right)^2 + \left(Q_{t,j}^{\mathrm{SOP}}\right)^2 \leq 2 \frac{P_{t,j}^{\mathrm{SOP,loss}}}{\sqrt{2}A_j^{\mathrm{SOP}}} \frac{P_{t,j}^{\mathrm{SOP,loss}}}{\sqrt{2}A_j^{\mathrm{SOP}}} \tag{41}$$

$$\left(P_{t,i}^{\mathrm{a}}\right)^2 + \left(Q_{t,i}^{\mathrm{a}}\right)^2 \leq 2 \frac{S_i^{\mathrm{a}}}{\sqrt{2}} \frac{S_i^{\mathrm{a}}}{\sqrt{2}}, \mathrm{a} \in \{\mathrm{SOP, DG}\} \tag{42}$$

As for the nonlinear threshold function in (11), auxiliary variable $Aux_{t,i}$ is introduced to express the extent of voltage deviation. Constraint (11) can be linearized as:

$$f_V = \sum_{t=1}^{N_T} \sum_{i=1}^{N_N} Aux_{t,i} \tag{43}$$

And some equivalent constraints are added as follows [23].

$$Aux_{t,i} \geq v_{t,i} - \left(\bar{U}_{\mathrm{thr}}\right)^2 \tag{44}$$

$$Aux_{t,i} \geq -v_{t,i} + \left(\underline{U}_{\mathrm{thr}}\right)^2 \tag{45}$$

$$Aux_{t,i} \geq 0 \tag{46}$$

As a result of the variable substitution, the OLTC operation constraint (23) can be expressed as:

$$v_{t,i} = k_{t,ij}^2 \, v_{t,j} \tag{47}$$

The number of tap steps $K_{t,ij}$ is an integer variable, which can be represented by a set of binary variables as follows [30]:

$$K_{t,ij} = \sum_{k=0}^{2\bar{K}_{ij}} \left[\left(k - \bar{K}_{ij} \right) b_{t,ij,k} \right] \tag{48}$$

$$\sum_{k=0}^{2\bar{K}_{ij}} b_{t,ij,k} = 1, \ b_{t,ij,k} \in \{0,1\} \tag{49}$$

Then, substituting constraints (24) and (48) into (47), it will yield:

$$v_{t,i} = \sum_{k=0}^{2\bar{K}_{ij}} \left[\left(k_{ij,0} + \left(k - \bar{K}_{ij} \right) \Delta k_{ij} \right)^2 v_{t,j} b_{t,ij,k} \right] \tag{50}$$

The nonlinear product $v_{t,j} b_{t,ij,k}$ is represented by the variable $v_{t,ij,k}^c$. And the additional constraints are added as follows.

$$v_{t,i} = \sum_{k=0}^{2\bar{K}_{ij}} \left[\left(k_{ij,0} + \left(k - \bar{K}_{ij} \right) \Delta k_{ij} \right)^2 v_{t,ij,k}^c \right] \tag{51}$$

$$(\underline{U}_j)^2 b_{t,ij,k} \le v_{t,ij,k}^c \le (\bar{U}_j)^2 b_{t,ij,k} \tag{52}$$

$$(\underline{U}_j)^2 \left(1 - b_{t,ij,k} \right) \le v_{t,j} - v_{t,ij,k}^c \le (\bar{U}_j)^2 \left(1 - b_{t,ij,k} \right) \tag{53}$$

As for the absolute term denoting the changes of tap steps in (10) and (25), auxiliary variables $K_{t,ij}^+$ and $K_{t,ij}^-$ are introduced to represent and linearize it as follows [31]:

$$\sum_{t=1}^{N_T} \left(K_{t,ij}^+ + K_{t,ij}^- \right) \le \bar{\Delta}^{\text{OLTC}} \tag{54}$$

$$K_{t,ij} - K_{t-1,ij} = K_{t,ij}^+ - K_{t,ij}^- \tag{55}$$

$$K_{t,ij}^+ \ge 0, \ K_{t,ij}^- \ge 0 \tag{56}$$

Similarly, constraints (57)–(59) represent a linear equivalent to the absolute term in (10) and (28), which denotes the variation of CB units in operation.

$$\sum_{t=1}^{N_T} \left(N_{t,i}^+ + N_{t,i}^- \right) \le \bar{\Delta}^{\text{CB}} \tag{57}$$

$$N_{t,i}^{\text{CB}} - N_{t-1,i}^{\text{CB}} = N_{t,i}^+ - N_{t,i}^- \tag{58}$$

$$N_{t,i}^+ \ge 0, \ N_{t,i}^- \ge 0 \tag{59}$$

And the (10) is expressed in a linear form:

$$f_{\text{act}} = \sum_{ij \in \Omega_O} \sum_{t=1}^{N_T} \left(C_{\text{tap}} \left(K_{t,ij}^+ + K_{t,ij}^- \right) \right)$$
$$+ \sum_{i=1}^{N_N} \sum_{t=1}^{N_T} \left(C_{\text{cap}} \left(N_{t,i}^+ + N_{t,i}^- \right) \right) \tag{60}$$

Now, after the linearization and conic relaxation, the original MINLP model is converted into the following MISOCP model.

$$\min \ f = W_L \left(f_{\text{loss}} + f_{\text{switch}} \right) + W_V f_V$$

$$\text{s.t.} \begin{cases} (1), (4), (5), (16), (17), (20), (21), (24), (26), \\ (27), (29), (33)-(46), (48), (49), (51)-(60) \end{cases} \tag{61}$$

As for the above MISOCP model, the key inputs consist of the network topology, locations and capacities of the loads and DGs, and parameters of the VAR regulation devices. The objective function and constraints of the model are shown in (61). The decision variables in this model involve not only the continuous active and reactive power outputs of SOPs, but also involve the discrete tap steps of OLTCs and switchable units of CBs. The outputs include the overall system operational cost, voltage deviation, operation strategies of the VAR regulation devices, and the power flow results of ADNs.

By linearization and conic relaxation, the coordinated VVC problem is converted into an MISOCP model which can efficiently obtain the global optimal solution of the proposed formulation [28]. It should be noted that there exists a relatively small gap between this solution and the solution to the original MINLP model, which is mainly caused by the conic relaxation deviation. Reference [32] has proved that the conic relaxation is exact with no gap if the objectives strictly increase in power injection or branch current. As this paper considers a comprehensive objective function of the minimum total operational cost and voltage deviation, the conic relaxation results in a small gap between the two models. However, previous studies have shown that the conic relaxation still has sufficient accuracy for distribution networks under some mild conditions [33], which are satisfied in the proposed MISOCP formulation. And the conic relaxation has been applied and validated in many works, i.e., optimal power flow [34], total supply capability evaluation [35], and supply restoration [36]. Thus, through the proposed MISOCP formulation, a good quality solution with a relaxed optimality gap can be efficiently obtained [37].

As the equality constraint (15) is relaxed to inequality constraint (39), the infinite norm of relaxation deviation [35] is defined to evaluate the accuracy of the conic relaxation.

$$\text{gap} = \left\| l_{t,ij} - \frac{P_{t,ij}^2 + Q_{t,ij}^2}{v_{t,i}} \right\|_{\infty} \tag{62}$$

If the gap value is small enough, the conic relaxation can be regarded as accurate for model conversion. Otherwise, the
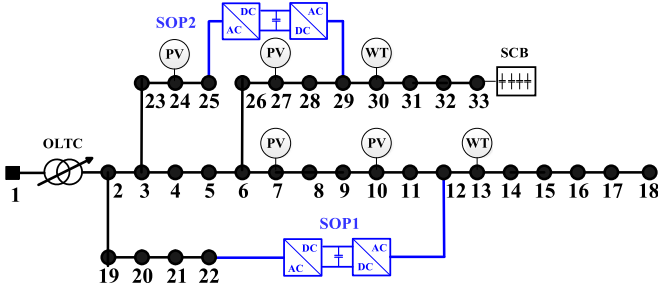
Fig. 2.   Structure of the modified IEEE 33-node system.

Fig. 3.   Daily operation curves of DGs and loads.

TABLE I
BASIC INSTALLATION PARAMETERS OF DGS

Parameters	Wind turbines		Photovoltaics			
Location	13	30	7	10	24	27
Capacity (kVA)	1000	1000	500	500	300	400

gap can also be constrained to the predefined error precision by adding the increasingly tight cuts to the conic relaxation [38].

IV. CASE STUDIES AND ANALYSIS

In this section, the modified IEEE 33-node and 123-node systems are used to demonstrate the effectiveness and efficiency of the coordinated VVC method based on SOP. Firstly, the performance of the VVC method involving the coordination of multiple regulation devices is analyzed on the modified IEEE 33-node system. Then, the test cases are carried out on the IEEE 123-node system to verify the scalability of the proposed method. By comparing with the algorithm packages in GAMS, the computation efficiency of the coordinated VVC method based on MISOCP model is verified.

The proposed method in this paper was implemented in the YALMIP optimization toolbox [39] with MATLAB R2013a, and solved by IBM ILOG CPLEX 12.6. The computation is performed on a PC with an Intel Xeon CPU E5-1620 @3.70 GHz processor and 32 GB RAM.

A. Modified IEEE 33-Node System

The modified IEEE 33-node test system is presented in Fig. 2, of which the rated voltage level is 12.66 kV. And the detailed parameters are provided in [40].

In order to consider the impact of high penetration of DGs on ADNs, two wind turbines and four photovoltaic generators are integrated into the networks, of which the total active power reaches to a 100% DG penetration level. All the DGs are operated at a unit power factor without considering the localized reactive power support of DGs [41]. The basic installation parameters are shown in Table I.

Taking hourly time step over a day, the daily DGs and loads operation curves are obtained by forecasting, as shown in Fig. 3.
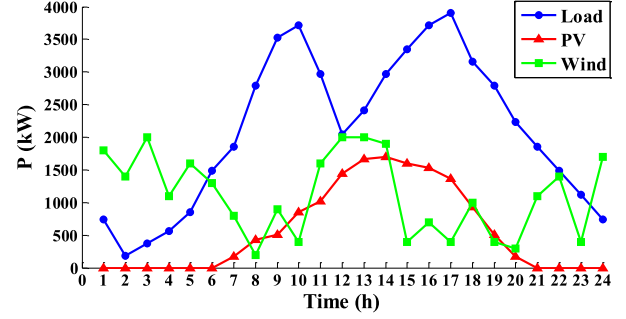
Two groups of SOP with a capability of 500 kVA are installed between the nodes 12 and 22, as well as the nodes 25 and 29, of which the upper reactive power limits are 300 kVar. It is assumed that the loss coefficient of each inverter for SOP is 0.02 [20], [42]. There is an OLTC with ten tap steps and a regulation of 1% per tap between the node 1 and 2. Besides, the switchable CBs of 150 kVar with five units are connected to node 33. Considering that frequent switching actions bring security risks to the operation, it is assumed that $\bar{\Delta}^{\text{OLTC}}$ for OLTC and $\bar{\Delta}^{\text{CB}}$ for CBs are all set as 4 times per day.

The weight coefficients W_L and W_V are determined as 0.833 and 0.167 by AHP [23]. The cost coefficient associated with active power losses C_{loss}, namely the basic cost of electricity buying from the upper grid, is assumed as 0.08$/kWh [43], [44] in this paper. The cost coefficients associated with variation of the tap steps C_{tap} and the CB units C_{cap} are set as 1.40 $/time and 0.24 $/time respectively [45], [46], which can be adjusted according to the switching risk assessment of DSO. It is assumed that the upper/lower limits of statutory voltage range $\bar{U} = 1.05$ p.u and $\underline{U} = 0.95$ p.u. And the desired voltage range is set from 0.97 p.u. to 1.03 p.u., which is also the margin of threshold in the voltage interval control strategy.

B. Optimization Results Analysis

Considering the coordination of multiple VAR regulation devices, the system voltage can be maintained at the desired level, while improving the operational efficiency of ADNs. Three scenarios are used to compare and analyze the performance of the coordinated VVC method based on SOP, and the optimization results are shown from Figs. 4 to 6.

Scenario I: Considering the cooperation of multiple VAR regulation devices, the coordinated VVC is conducted.

Scenario II: Only based on the conventional adjusting of OLTC and switching of CBs, the VVC is conducted.

Scenario III: Without the VVC in the system.

It can be seen from Fig. 4 that the operation strategies of SOP are accordance with the power supply and demand of ADNs in Scenario I. The high penetration of DGs makes a wide fluctuation of power flow. During the hours 6:00–10:00 and 14:00–20:00, DGs can't supply the high electricity demand. The two groups of SOP transmit the active power into node 12 and node 29 to alleviate the power demand of the system.
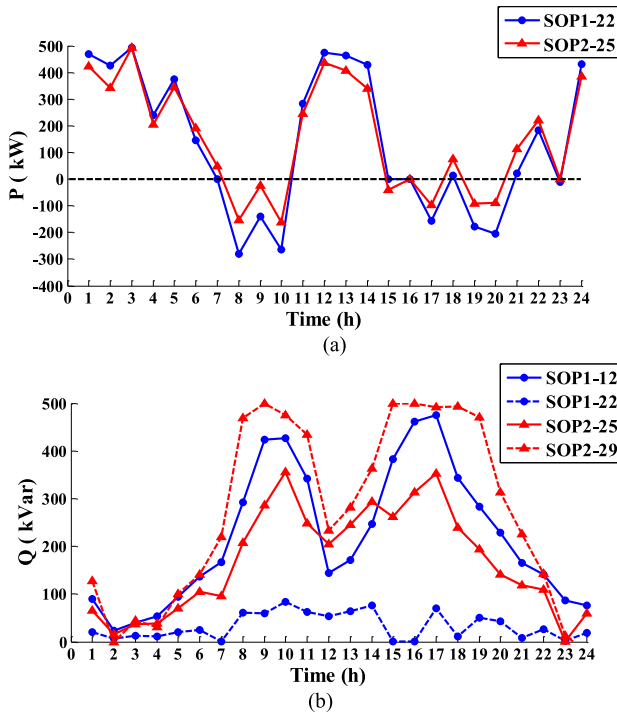
Fig. 4.   Scheduling strategies of SOP in Scenario I. (a) Active power transmission of SOP. (b) Reactive power compensation of SOP.
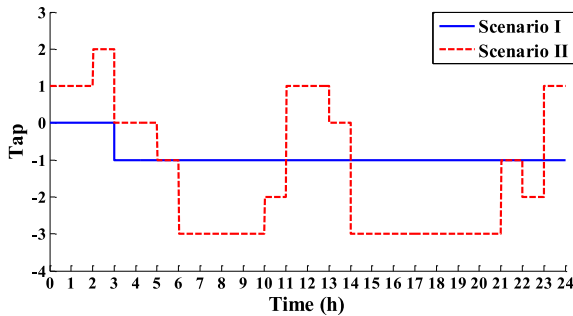

Fig. 5.   Tap movements of the OLTC in Scenario I and II.
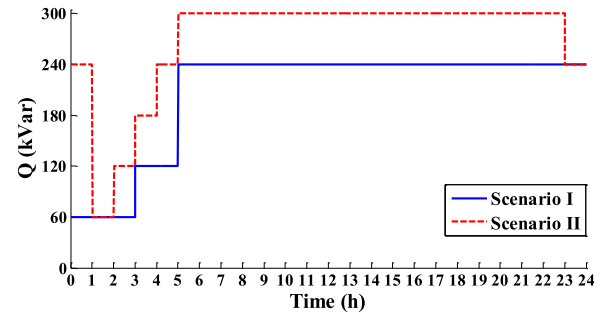

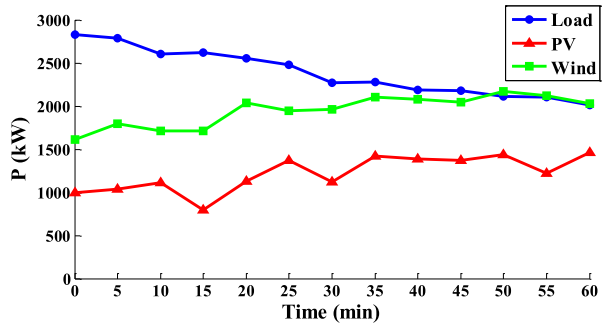Fig. 6.   Total reactive power injected by CBs in Scenario I and II.

Fig. 7.   DG outputs and loads fluctuation in one hour.

TABLE II
OPTIMIZATION RESULTS OF EACH SCENARIO

Optimization results	Scenario I	Scenario II	Scenario III
Cost of active power losses ($/day)	50.17	87.93	111.27
Cost of switching operation ($/day)	2.36	32.28	0
Total system operational cost ($/day)	52.53	120.21	111.27
Extent of voltage deviations (p.u.)	0.01	0.02	3.43

However, as the abundant outputs of DGs are far more than the load demands in the hours 11:00–13:00 and 21:00–5:00, the two groups of SOP are scheduled to inversely transmit the active power into node 22 and node 25 in order to smooth the power fluctuations as much as possible.

SOP cooperates with multiple VAR regulation devices in Scenario I. SOP adjusts the active and reactive power flow and timely responds to the voltage volatility caused by DGs. Compared to Scenario II, the switching devices comprising OLTC and CBs regulate the VAR in the long time scale to avoid frequently actions, which effectively lower the security risks of system operation, as shown in Figs. 5 and 6.

Taking a time period 11:00–12:00 in one day as example, the fluctuation curves of DG outputs and loads are shown in Fig. 7, and the time interval is assumed as 5 min.

The tap position of OLTC is kept unchanged at –1 and the number of CB units in operation remains 4 in this time period.

SOP dynamically controls its active and reactive power flow in every 5 min to rapidly respond to the fluctuations caused by DGs and loads, as shown in Fig. 8. Thus the VAR regulation can be carried out in the short time scale, effectively alleviating the voltage volatility in ADNs, as shown in Fig. 9.

Compared with the other two scenarios, the coordinated VVC is implemented in Scenario I based on SOP. The voltage is controlled within the desired range of 0.97–1.03 p.u., flattening the voltage profile of feeders. When the voltage violation occurs, various VAR regulation devices cooperate to eliminate it effectively. The voltage profiles of node 18 and the maximum and minimum system voltages are shown in Figs. 10 and 11, respectively.

The optimization results of three scenarios are listed in Table II. It shows that the improvements of operation costs reduction are much more significant in Scenario I.

Based on the above analysis, the proposed coordinated VVC method using SOP eliminates the voltage violations and decreases the system operation costs, ensuring the operational security and economy of ADNs simultaneously.

The gap values in each time period of Scenario I and II are shown in Fig. 12. It can be seen that the maximum gap values
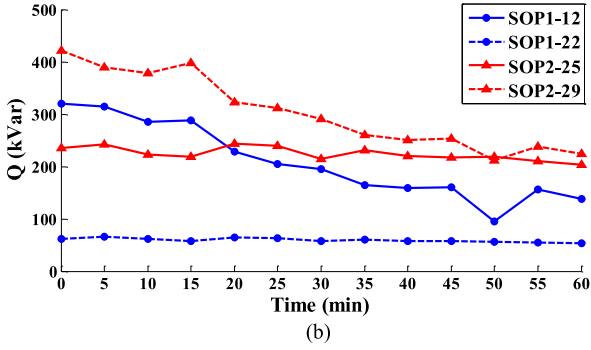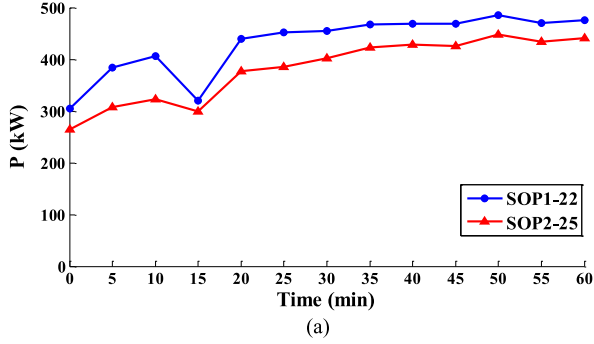
Fig. 8. Scheduling strategies of SOP in one hour. (a) Active power transmission of SOP. (b) Reactive power compensation of SOP.
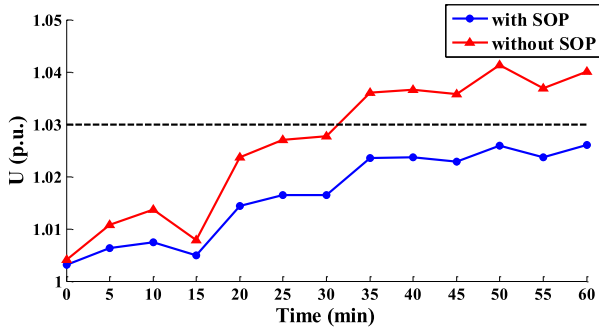

Fig. 9. Voltage profiles of node 18 with and without SOP in one hour.
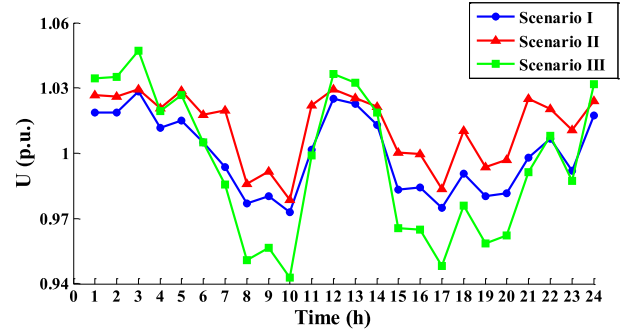

Fig. 10. Voltage profile of node 18 in three scenarios.

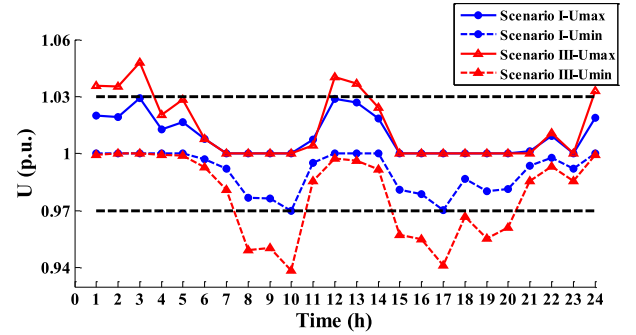

Fig. 11. Maximum and minimum system voltages in Scenario I and III.

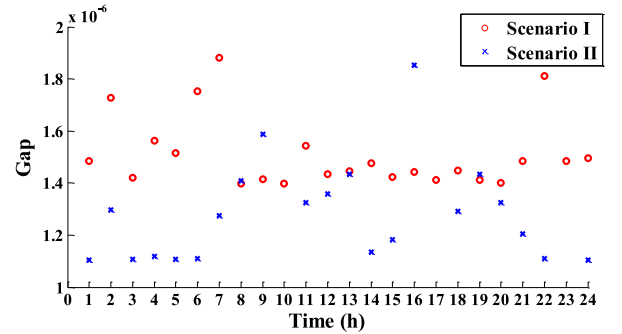Fig. 12. Maximum gap values in each time period of Scenario I and II.

in both scenarios are all with a 1.0^{e-6} level, which are small enough to be regarded as accurate. So the proposed MISOCP model calculates the coordinated VVC problem with acceptable accuracy.

The main motivation for using the MISOCP model is to obtain the optimal solution of MINLP model as close as possible with a high computational efficiency.

C. Cost-Benefit Analysis of SOP

The application of SOP will significantly facilitate the operation of ADNs, including power loss reduction, voltage profile improvement, increasing the DG hosting capacity, as well as fault isolation and supply restoration under abnormal condition [13], [20]. The cost-benefit analysis of SOP is briefly and simply addressed from the economic perspective in Scenario I.

The costs associated with SOP include the equipment investment cost and maintenance cost. The benefits brought by SOP are mainly from saving the system operational cost by the reduction of active power losses and the switching operation cost. The model of cost-benefit analysis shows from (63) to (66).

1) C^{INV}: SOP fixed investment cost

$$C^{\mathrm{INV}} = \sum_{i=1}^{N_N} c^{\mathrm{SOP}} S_i^{\mathrm{SOP}} \tag{63}$$

Where c^{SOP} is the investment cost per unit capacity and S_i^{SOP} denotes the installed SOP capacity connected to node i.

2) C^{MAI}: SOP annual maintenance cost

$$C^{\mathrm{MAI}} = \eta \sum_{i=1}^{N_N} c^{\mathrm{SOP}} S_i^{\mathrm{SOP}} \tag{64}$$

TABLE III
PARAMETERS OF COST-BENEFIT ANALYSIS

Parameters	Value
SOP economical service life (year)	20
SOP unit capacity investment ($/kVA)	308.8
Installation of SOP capacity (kVA)	1000
Coefficient of annual maintenance cost	0.01

TABLE IV
RESULTS OF COST-BENEFIT ANALYSIS

Cost-benefit analysis	Scenario I	Scenario II	Reduction
Annual cost of power losses ($)	18 312.05	32 094.45	13 782.40
Annual cost of switching operation ($)	861.40	11 782.20	10 920.80
Annual SOP maintenance cost ($)	3088.00	0.00	−3088.00
Annual total cost of system operation ($)	22 261.45	43 876.65	21 615.20

Where η is the coefficient of the annual maintenance cost.

3) B^{LOSS}: Annual cost of the active power losses

$$
B^{\mathrm{LOSS}} = 365 \cdot C_{\mathrm{loss}} \cdot \left(\sum_{t=1}^{N_T} \sum_{ij \in \Omega_b} r_{ij} I_{t,ij}^2 \Delta t \right.
$$
$$
\left. + \sum_{t=1}^{N_T} \sum_{i=1}^{N_N} P_{t,i}^{\mathrm{SOP,loss}} \Delta t \right) \quad (65)
$$

4) B^{OPE}: Annual cost of the switching operation

$$
B^{\mathrm{OPE}} = 365 \cdot \left(\sum_{ij \in \Omega_O} \sum_{t=1}^{N_T} (C_{\mathrm{tap}} |K_{t,ij} - K_{t-1,ij}|) \right.
$$
$$
\left. + \sum_{i=1}^{N_N} \sum_{t=1}^{N_T} \left(C_{\mathrm{cap}} |N_{t,i}^{\mathrm{CB}} - N_{t-1,i}^{\mathrm{CB}}| \right) \right) \quad (66)
$$

As for the modified IEEE 33-node system, the parameters of cost-benefit analysis [22] are shown in Table III.

Compared with the optimization results of Scenario II in Table II, the cost-benefit analysis under Scenario I are shown in Table IV.

Table IV shows that the application of SOP in Scenario I has better economic benefits. Compared with Scenario II, the annual system operational cost of Scenario I is reduced by $21 615.20 (reduction of 49.3 percent). It will take 14.29 years to cover the SOP investment cost in Scenario I. With the decreasing in the price of power electronic devices, the economic benefits brought by SOP will become more obvious.

D. Modified IEEE 123-Node System

The modified IEEE 123-node system is adopted to verify the scalability of proposed method on the large-scale ADNs, as shown in Fig. 13. The detailed parameters can refer to [36].

Three wind turbines and six photovoltaic generators are integrated into the networks, of which the basic installation parameters are shown in Table V. Two groups of SOP are installed be-
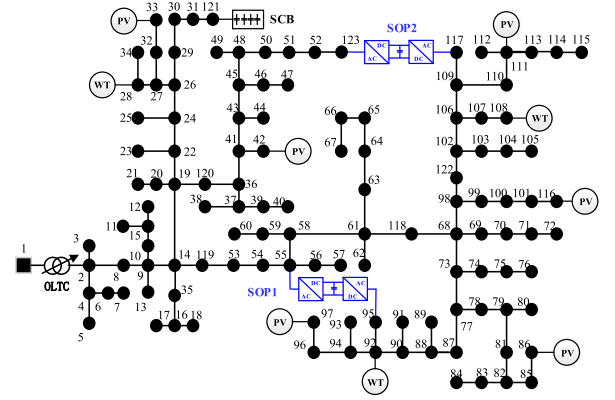

Fig. 13. Structure of the modified IEEE 123-node system.

TABLE V
BASIC INSTALLATION PARAMETERS OF DGs

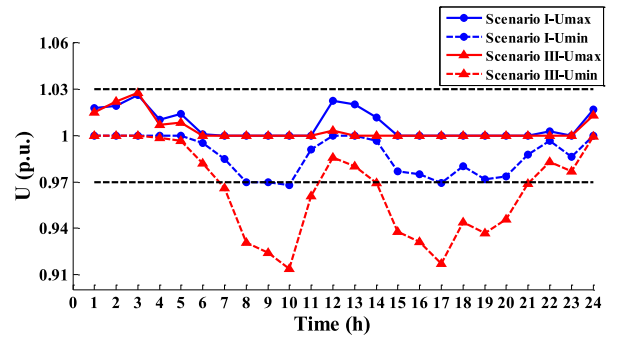| Parameters	Wind turbines			Photovoltaics					
Location	28	92	108	33	42	86	97	111	116
Capacity (kVA)	1000	1000	1000	300	300	200	200	500	500

Fig. 14. Maximum and minimum system voltages in Scenario I and III.

tween the nodes 55 and 95, as well as nodes 117 and 123. There is an OLTC between the node 1 and 2. Besides, the switchable CBs are installed at node 121. The parameters of above regulation devices are set to the same value as the IEEE 33-node system.

Based on the coordination of various VAR regulation devices, the voltage is maintained within the desired range and the voltage deviation is effectively reduced. The maximum and minimum voltages of the whole system in Scenario I and III adopted in Section IV-B are shown in Fig. 14.

Similar to the conclusions in Section IV-B, by the coordination of SOP and multiple VAR regulation devices, the voltage fluctuations caused by high penetration of DGs are effectively mitigated and the economic performance of the ADNs is improved simultaneously.

TABLE VI
PERFORMANCE COMPARISON OF THE PROPOSED MODEL AND KNITRO

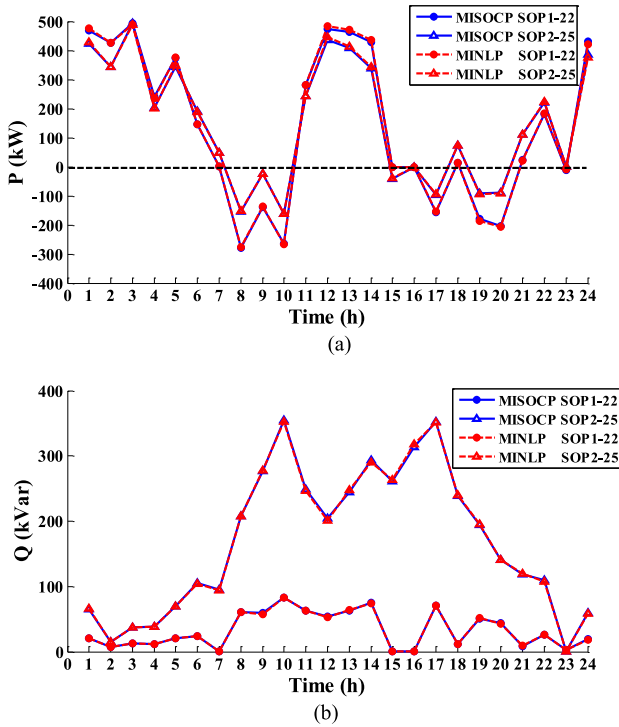| Test case	Scale of problem	Optimization model/Solver	Time (s)	Operational costs ($/day)	Voltage deviation
IEEE 33-node	Variables: 4656	MISOCP/CPLEX	62.76	52.53	0.01
	Constraints: 10 298	MINLP/KNITRO	364.21	52.51	0.01
IEEE 123-node	Variables: 13 512	MISOCP/CPLEX	1207.14	75.61	0.04
	Constraints: 27 866	MINLP/KNITRO	Divergent	–	–

Fig. 15. Optimal strategies of SOP with the MISOCP and MINLP models. (a) Optimal active power transmission of SOP. (b) Optimal reactive power compensation of SOP.

Fig. 16. Active power losses in each time period.

E. Algorithm Validation

To verify the effectiveness and accuracy of the proposed method based on MISOCP, MINLP solver KNITRO [47] in GAMS is used to solve the original MINLP model comprising (1)–(29) as a reference. KNITRO is an optimization package based on KKT algorithm and interior point method, which ensures a high quality solution and has been widely applied in solving the MINLP problem. Table VI compares the results and performances of the proposed model and KNITRO.

Table VI shows that compared with KNITRO, the proposed MISOCP model promotes the computing speed while solving the problem accurately because of the linearization and convex relaxation of the original model. With a sharp increasing in problem scale caused by more time periods and larger system, KNITRO package may bring the curse of dimensionality in solving large-scale MINLP problem, and even can't guarantee the convergence. The MISOCP model proposed in this paper
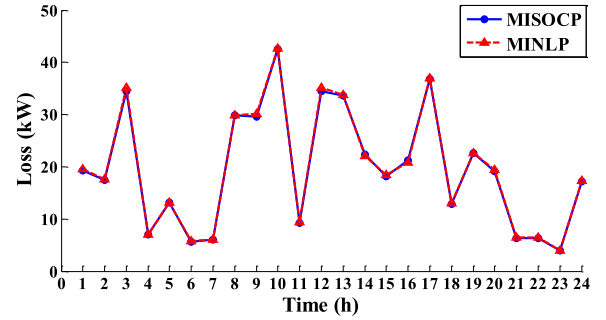
still shows improved convergence and efficiency by reducing the complexity of the problem.

To further illustrate the effectiveness and accuracy of the proposed MISOCP model, time-series power flow simulations are conducted based on the operation strategies from the both models. And the time-series simulation results for the modified IEEE 33-node system are shown in Figs. 15 and 16.

As shown in Figs. 15 and 16, the optimization results obtained by the two models keep nearly the same, verifying the effectiveness of the proposed MISOCP model.

V. CONCLUSION

This paper presents a coordinated VVC method based on SOP to minimize the operation costs and improve the voltage profile of ADNs. Considering the cooperation of SOP and multiple VAR regulation devices, a time-series optimization model of coordinated VVC is developed, in which the SOP, OLTC and switchable CBs are all formulated as controllable devices. Then the original large-scale MINLP model is converted into the MISOCP model via the linearization and conic relaxation. The optimization results show that by applying the SOP-based coordinated VVC method, the system voltage is maintained at the desired level while the operational efficiency is significantly improved. Based on MISOCP, the proposed method guarantees global optimality and has a moderate computational burden, and it is suitable for the efficient VVC of large-scale ADNs with high penetration of DGs.

Taking the characteristics of DGs and network topology changing into account, the determination of optimal siting and sizing for SOP needs to be further considered due to its relatively high investment. Besides, facing a larger-scale complicated ADN, a completely centralized approach may not be applicable because of its computation and communication

burden. Regulating the voltage and VAR based on SOP in a partly distributed manner is also worthy of further research.

REFERENCES

[1] J. P. Lopes and N. Hatziargyriou, "Integrating distributed generation into electric power systems: A review of drivers, challenges and opportunities," *Electr. Power Syst. Res.*, vol. 77, no. 9, pp. 1189–1203, 2007.

[2] A. C. Rueda-Medina and A. Padilha-Feltrin, "Distributed generators as providers of reactive power support—A market approach," *IEEE Trans. Power Syst.*, vol. 28, no. 1, pp. 490–502, Feb. 2013.

[3] K. Kuroda and H. Magori, "A hybrid multi-objective optimization method considering optimization problems in power distribution systems," *J. Mod. Power Syst. Clean Energy*, vol. 3, no. 1, pp. 41–50, 2015.

[4] P. Hallberg *et al.*, "Active distribution system management a key tool for the smooth integration of distributed generation," Eurelectric TF Active System Management Paper, 2013.

[5] M. Tan, C. Han, and X. Zhang, "Hierarchically correlated equilibrium Q-learning for multi-area decentralized collaborative reactive power optimization," *CSEE J. Power Energy Syst.*, vol. 2, no. 3, pp. 65–72, 2016.

[6] Q. Ai, S. Fan, and L. Piao, "Optimal scheduling strategy for virtual power plants based on credibility theory," *Protection Control Mod. Power Syst.*, vol. 1, no. 1, pp. 1–8, 2016.

[7] J. Barr and R. Majumder, "Integration of distributed generation in the volt/var management system for active distribution networks," *IEEE Trans. Smart Grid*, vol. 6, no. 2, pp. 576–586, Mar. 2014.

[8] P. D. Ferreira, P. Carvalho, and L. A. Ferreira, "Distributed energy resources integration challenges in low-voltage networks: Voltage control limitations and risk of cascading," *IEEE Trans. Sustain. Energy*, vol. 4, no. 1, pp. 82–88, Jan. 2013.

[9] Y. P. Agalgaonkar, B. C. Pal, and R. A. Jabr, "Distribution voltage control considering the impact of PV generation on tap changers and autonomous regulators," *IEEE Trans. Power Syst.*, vol. 29, no. 1, pp. 182–192, Jan. 2014.

[10] M. B. Liu, C. A. Canizares, and W. Huang, "Reactive power and voltage control in distribution systems with limited switching operations," *IEEE Trans. Power Syst.*, vol. 24, no. 1, pp. 427–436, Feb. 2009.

[11] J. M. Bloemink and T. C. Green, "Benefits of distribution-level power electronics for supporting distributed generation growth," *IEEE Trans. Power Del.*, vol. 28, no. 2, pp. 911–919, Apr. 2013.

[12] W. Cao, J. Wu, and N. Jenkins, "Operating principle of soft open points for electrical distribution network operation," *Appl. Energy*, vol. 164, pp. 245–257, 2016.

[13] C. Long, J. Wu, and L. Thomas, "Optimal operation of soft open points in medium voltage electrical distribution networks with distributed generation," *Appl. Energy*, vol. 184, pp. 427–437, 2016.

[14] F. Capitanescu and I. Bilibin, "A comprehensive centralized approach for voltage constraints management in active distribution grid," *IEEE Trans. Power Syst.*, vol. 29, no. 2, pp. 933–942, Mar. 2014.

[15] A. Rajan and T. Malakar, "Optimal reactive power dispatch using hybrid Nelder-Mead simplex based firefly algorithm," *Int. J. Electr. Power Energy Syst.*, vol. 66, pp. 9–24, 2015.

[16] N. Daratha and B. Das, "Coordination between OLTC and SVC for voltage regulation in unbalanced distribution system distributed generation," *IEEE Trans. Power Syst.*, vol. 29, no. 1, pp. 289–299, Jan. 2014.

[17] M. Farivar, R. Neal, and C. Clarke, "Optimal inverter VAR control in distribution systems with high PV penetration," in *Proc. IEEE Power Energy Soc. Gen. Meeting*, 2012, pp. 1–7.

[18] Z. Tian, W. Wu, and B. Zhang, "Mixed-integer second-order cone programing model for VAR optimization and network reconfiguration in active distribution networks," *IET Gener. Transm. Distrib.*, vol. 10, no. 8, pp. 1938–1946, 2016.

[19] A. Gabash and P. Li, "Active-reactive optimal power flow in distribution networks with embedded generation and battery storage," *IEEE Trans. Power Syst.*, vol. 27, no. 4, pp. 2026–2035, Nov. 2012.

[20] W. Cao, J. Wu, and N. Jenkins, "Benefits analysis of soft open points for electrical distribution network operation," *Appl. Energy*, vol. 165, pp. 36–47, 2016.

[21] I. Konstantelos, S. Giannelos, and G. Strbac, "Strategic valuation of smart grid technology options in distribution networks," *IEEE Trans. Power Syst.*, vol. 32, no. 2, pp. 1293–1303, Mar. 2017.

[22] C. Wang, G. Song, and P. Li, "Optimal siting and sizing of soft open points in active electrical distribution networks," *Appl. Energy*, vol. 189, pp. 301–309, 2017.

[23] N. Mostafa, C. Rachid, and P. Mario, "Optimal allocation of dispersed energy storage systems in active distribution networks for energy balance and grid support," *IEEE Trans. Power Syst.*, vol. 29, no. 5, pp. 2300–2310, Sep. 2014.

[24] M. Nick, R. Cherkaoui, and M. Paolone, "Optimal siting and sizing of distributed energy storage systems via alternating direction method of multipliers," *Int. J. Electr. Power Energy Syst.*, vol. 72, pp. 33–39, 2015.

[25] M. E. Baran, "Optimal capacitor placement on radial distribution systems," *IEEE Trans. Power Del.*, vol. 4, no. 1, pp. 725–734, Jan. 1989.

[26] E. D. Andersen, C. Roos, and T. Terlaky, "On implement a primal-dual interior point methods for conic quadratic optimization," *Math. Program.*, vol. 95, no. 2, pp. 249–277, 2003.

[27] C. Huang, F. Li, T. Ding, Z. Jin, and X. Ma, "Second-order cone programming-based optimal control strategy for wind energy conversion systems over complete operating regions," *IEEE Trans. Sustain. Energy*, vol. 6, no. 1, pp. 263–271, Jan. 2015.

[28] S. H. Low, "Convex relaxation of optimal power flow, I: Formulations and relaxations," *IEEE Trans. Control Netw. Syst.*, vol. 1, no. 1, pp. 15–27, Mar. 2014.

[29] M. Farivar and S. H. Low, "Branch flow model: Relaxations and convexification-Part I," *IEEE Trans. Power Syst.*, vol. 28, no. 3, pp. 2554–2564, Aug. 2013.

[30] T. Ding, S. Liu, and W. Yuan, "A two-stage robust reactive power optimization considering uncertain wind power integration in active distribution networks," *IEEE Trans. Sustain. Energy*, vol. 7, no. 1, pp. 301–311, Jan. 2016.

[31] L. H. Macedo, J. F. Franco, and M. J. Rider, "Optimal operation of distribution networks considering energy storage devices," *IEEE Trans. Smart Grid*, vol. 6, no. 6, pp. 2825–2836, Nov. 2015.

[32] J. Lavaei and S. H. Low, "Zero duality gap in optimal power flow problem," *IEEE Trans. Power Syst.*, vol. 27, no. 1, pp. 92–107, Feb. 2012.

[33] L. Gan, N. Li, U. Topcu, and S. H. Low, "Exact convex relaxation of optimal power flow in radial networks," *IEEE Trans. Autom. Control*, vol. 60, no. 1, pp. 72–87, Jan. 2015.

[34] M. Baradar, M. R. Hesamzadeh, and M. Ghandhari, "Second-order cone programming for optimal power flow in VSC-type AC-DC grids," *IEEE Trans. Power Syst.*, vol. 28, no. 4, pp. 4282–4291, Nov. 2013.

[35] K. Chen, W. Wu, and B. Zhang, "A method to evaluate total supply capability of distribution systems considering network reconfiguration and daily load curves," *IEEE Trans. Power Syst.*, vol. 31, no. 3, pp. 2096–2104, Oct. 2016.

[36] K. Chen, W. Wu, and B. Zhang, "Robust restoration method for active distribution networks," *IEEE Trans. Power Syst.*, vol. 31, no. 5, pp. 4005–4015, Sep. 2016.

[37] R. A. Jabr, R. Singh, and B. C. Pal, "Minimize loss network reconfiguration using mixed-integer convex programming," *IEEE Trans. Power Syst.*, vol. 27, no. 2, pp. 1106–1115, May 2012.

[38] S. Y. Abdelouadoud and R. Girard, "Optimal power flow of a distribution system based on increasingly tight cutting planes added to a second order cone relaxation," *Int. J. Electr. Power Energy Syst.*, vol. 69, pp. 9–17, 2015.

[39] J. Lofberg, "Yalmip: A toolbox for modeling and optimization in MATLAB," in *Proc. 2004 IEEE Int. Conf. Robot. Autom.*, 2004, pp. 284–289.

[40] M. E. Baran and F. F. Wu, "Network reconfiguration in distribution systems for loss reduction and load balancing," *IEEE Trans. Power Del.*, vol. 4, no. 2, pp. 1401–1407, Apr. 1989.

[41] I. Džafić, R. A. Jabr, E. Halilovic, and B. C. Pal, "A sensitivity approach to model local voltage controllers in distribution networks," *IEEE Trans. Power Syst.*, vol. 29, no. 3, pp. 1419–1428, May 2014.

[42] "PCS 6000 for large wind turbines: Medium voltage, full power converters up to 9 MVA," ABB, Brochure 3BHS351272 E01 Rev. A, 2012. [Online]. Available: http://new.abb.com/docs/default-source/ewea-doc/ pcs6000wind.pdf.

[43] D. Dallinger, J. Link, and M. Buttner, "Smart grid agent: Plug-in electric vehicle," *IEEE Trans. Sustain. Energy*, vol. 5, no. 3, pp. 710–717, Jul. 2014.

[44] H. M. Al-Masri and M. Ehsani, "Feasibility investigation of a hybrid on-grid wind photovoltaic retrofitting system," *IEEE Trans. Ind. Appl.*, vol. 52, no. 3, pp. 1979–1988, May/Jun. 2016.

[45] J. W. Lamont and J. Fu, "Cost analysis of reactive power support," *IEEE Trans. Power Syst.*, vol. 14, no. 3, pp. 890–898, Aug. 1999.

[46] T. Malakar and S. K. Goswami, "Active and reactive dispatch with minimum control movements," *Int. J. Electr. Power Energy Syst.*, vol. 44, no. 44, pp. 78–87, 2013.

[47] P. Bonami, L. T. Biegler, and A. R. Conn, "An algorithmic framework for convex mixed integer nonlinear programs," *Discrete Opt.*, vol. 5, no. 2, pp. 186–204, 2008.

Peng Li (M'11) received the B.S. and Ph.D. degrees in electrical engineering from Tianjin University, Tianjin, China, in 2004 and 2010, respectively.

He is currently an Associate Professor in the School of Electrical and Information Engineering, Tianjin University. His current research interests include distributed generation system and microgrid, smart distribution system, and transient simulation and analysis.

Haoran Ji (S'16) received the B.S. degree in electrical engineering from Tianjin University, Tianjin, China, in 2014, where he is currently working toward the Ph.D. degree in electrical engineering.

His current research interests include distribution system modelling and optimization.

Chengshan Wang (SM'11) received the Ph.D. degree in electrical engineering from Tianjin University, Tianjin, China, in 1991.

From 1994 to 1996, he was a Senior Academic Visitor with Cornell University, Ithaca, NY, USA. From 2001 to 2002, he was a Visiting Professor with the Carnegie Mellon University, Pittsburgh, PA. He is currently a Professor in the School of Electrical and Information Engineering, Tianjin University. He is the Director of the Key Laboratory of Smart Grid of Ministry of Education, Tianjin University. His current research interests include distribution system analysis and planning, distributed generation system and microgrid, and power system security analysis.

Dr. Wang is an editorial board member of *Applied Energy* and the *Journal of Modern Power Systems and Clean Energy*.

Jinli Zhao (M'11) received the Ph.D. degree in electrical engineering from Tianjin University, Tianjin, China, in 2007.

She is currently an Associate Professor in the School of Electrical and Information Engineering, Tianjin University. Her research interests include power system security and stability.

Guanyu Song received the B.S. degree in electrical engineering from Tianjin University, Tianjin, China, in 2012, where he is currently working toward the Ph.D. degree in electrical engineering.

His current research interests include optimal planning and operation of smart distribution system.
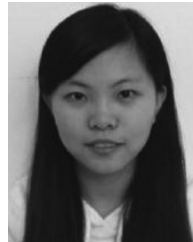
Fei Ding (M'14) received the Ph.D. degree from the Case Western Reserve University, Cleveland, OH, USA.

She joined the National Renewable Energy Laboratory as a Research Engineer in 2015. Her research interests include distribution system automation and optimization, distribution system modelling and simulation, renewable energy grid integration, microgrid, and smart grid.

Jianzhong Wu (M'14) received the Ph.D. degree from Tianjin University, Tianjin, China, in 2004.

From 2004 to 2006, he was with Tianjin University, where he is an Associate Professor. From 2006 to 2008, he was a Research Fellow with the University of Manchester, Manchester, U.K. He is currently a Professor with the Cardiff School of Engineering, Institute of Energy, London, U.K. His current research interests include energy infrastructure and smart grids.

Dr. Wu is a member of the Institution of Engineering and Technology and the Association for Computing Machinery.